Environmental Modelling & Software 58 (2014) 48–57

Contents lists available at ScienceDirect

Environmental Modelling & Software

journal homepage: www.elsevier.com/locate/envsoft

What is the effect of LiDAR-derived DEM resolution on large-scale watershed model results?☆

Ping Yang [a,*], Daniel P. Ames [b], André Fonseca [c], Danny Anderson [d], Rupesh Shrestha [e], Nancy F. Glenn [e], Yang Cao [a]

[a] Texas Institute for Applied Environmental Research, Tarleton State University, Stephenville, TX, USA
[b] Department of Civil and Environmental Engineering, Brigham Young University, Provo, UT, USA
[c] LSRE/LCM Department of Chemical Engineering, University of Porto, Porto, Portugal
[d] Idaho National Laboratory, Idaho Falls, ID, USA
[e] Department of Geosciences, Boise State University, Boise, ID, USA

ARTICLE INFO

Article history:
Received 10 January 2014
Received in revised form
1 April 2014
Accepted 3 April 2014
Available online

Keywords:
Hydrographic feature extraction
Hydrologic modeling
Stream networks
LiDAR
Digital elevation model
Terrain analysis

ABSTRACT

This paper examines the effect of raster cell size on hydrographic feature extraction and hydrological modeling using LiDAR derived DEMs. LiDAR datasets for three experimental watersheds were converted to DEMs at various cell sizes. Watershed boundaries and stream networks were delineated from each DEM and were compared to reference data. Hydrological simulations were conducted and the outputs were compared. Smaller cell size DEMs consistently resulted in less difference between DEM-delineated features and reference data. However, minor differences been found between streamflow simulations resulted for a lumped watershed model run at daily simulations aggregated at an annual average. These findings indicate that while higher resolution DEM grids may result in more accurate representation of terrain characteristics, such variations do not necessarily improve watershed scale simulation modeling. Hence the additional expense of generating high resolution DEM's for the purpose of watershed modeling at daily or longer time steps may not be warranted.

Software and data availability

Name	BASINS 4.0 (Better Assessment Science Integrating point & Non-point Sources) with a non-proprietary, open source, free GIS system, MapWindow (www.MapWindow.org)
Developer	U.S. EPA with AquaTerra Consultants and Idaho State University
Contact	http://www.aquaterra.com/contact/index.php
Availability and cost	The software is available for free download at USEPA (United States Environmental Protection Agency) website. Mapwindow is an open source programmable GIS (VB, C++, .NET, and Active × controls) that supports manipulation, analysis, and viewing of geospatial data and associated attribute data in several GIS data formats.

1. Introduction

Hydrologic simulation models and water resources planning tools often use hydrographic datasets (most importantly stream network polylines and watershed boundaries) which can be

☆ One sentence description: This paper explores the effects of LiDAR-derived DEM resolution on hydrographic features extraction used for streamflow simulation modeling.

* Corresponding author.
E-mail addresses: pingyang@tiaer.tarleton.edu, pingyang.whu@gmail.com (P. Yang).

http://dx.doi.org/10.1016/j.envsoft.2014.04.005
1364-8152/

derived from gridded (raster) digital elevation models (DEMs) using well-established terrain analysis techniques (Jenson and Domingue, 1988; Tarboton et al., 1991; Tarboton and Ames, 2001; Teng et al., 2008; Tesfa et al., 2011). DEMs used in these processes are derived from various sources including: manually surveyed topographic maps, aerial photogrammetry, interpolated global positioning system (GPS) points, and the NASA Shuttle Radar Topography Mission (Farr and Kobrick, 2000; Kinsey-Henderson and Wilkinson, 2013; Han et al., 2012). In recent years, another source of data from which DEMs can be derived has emerged in the form of Light Detection and Ranging data (LiDAR).

LiDAR technology offers a relatively efficient way to produce DEMs for high accuracy mapping applications. LiDAR sensors are capable of receiving multiple laser pulse returns which, when combined with precision GPS location data, can provide highly accurate and dense point sample measurements of terrain height and ground features (e.g. vegetation, built structures). In this way, LiDAR can be used to define a detailed representation of the earth's surface horizontally as well as vertically, making the LiDAR data source increasingly important for surface structure derivation and its application in hydrographic feature extraction. Indeed, channels extracted from a LiDAR-derived DEM have been shown to have a more complex morphology and correspond better with field-mapped networks than those derived from a conventionally produced DEM (Charrier and Li, 2012).

Murphy et al. (2007) suggests that when considering hydrologic modeling, DEM cell size has a greater impact on results than does the method by which the DEM was produced. Chow and Hodgson (2009) demonstrated that DEM resolution progressively affects the mean and deviation of slope within the range of 2–10 m. Shore et al. (2013) used a 5 m resolution DEM was to study subcatchment connectivity and found that detailed ditch data did not contribute significantly to improving results. These observations contribute to the primary question motivating the work presented here: What is the relationship between hydrographic derivatives (specifically watershed boundaries and stream network centerlines) and the cell size of the LiDAR-derived DEM? Furthermore, is there an optimal resolution of LiDAR-derived DEMs for hydrologic modeling? These questions are important because of the extensive use of DEM derived vector data features in both mapping and hydrologic modeling applications.

To address these questions, we produced several DEMs at different resolutions (cell-sizes) from LiDAR datasets from three different watersheds and delineated stream network centerlines and watershed boundary polygons for each watershed at each DEM resolution. The resulting vector data were then compared to best available reference datasets for each watershed. An assessment of the "correctness" of each extracted stream network is made through the use of longitudinal root mean square error (LRMSE), sinuosity deviation, and selected hydrographic parameters. To assess the effect of LiDAR-derived DEM cell size variation on streamflow simulation, a hydrologic model for a watershed was calibrated using input watershed and stream networks from each DEM resolution and resulting streamflow simulations were compared to observed data.

2. Background

Historically, literature on the effect of spatial scale on topographic modeling largely focuses on DEMs created by means other than LiDAR (Jenson, 1991; Moore, 1991; Tarboton et al., 1991; DeVantier and Feldman, 1993; Olivera, 2001). However, more recent studies include research on the effect of DEM resolution on hydrology-related parameters from LiDAR data (Kienzle, 2004; Vaze et al., 2010; Sørensen and Seibert, 2007). Tarboton et al. (1991) explored the length scale or drainage density for network derivation from traditional digital elevation data, and suggested criteria for determining the appropriate drainage density at which to extract networks from DEMs. Zhang and Montgomery (1994) found that increasing the grid size resulted in an increased mean topographic index because of increased contributing area and decreased slopes. Wolock and Price (1994) found that increasing grid size resulted in higher minimum, mean, variance, and skew of the topographic index distribution. Techniques for generating DEM data from LiDAR have been greatly improved in the last decade (Kraus and Pfeifer, 2001; Agarwal et al., 2006; Xiaoye, 2008). With respect to the use of the LiDAR-derived DEMs for hydrologic modeling, Murphy et al. (2007) compared stream network modeling results using LiDAR and photogrammetric derived digital elevation which reveals that a flow network modeled from the LiDAR-derived DEM was most accurate.

Kienzle (2004) investigated the effect of DEM raster resolution on first order, second order and compound terrain derivatives and identified an optimum grid cell size between 5 and 20 m, related to terrain complexity. Sørensen and Seibert (2007) also showed that the resolution and information content of a DEM has great influence on the computed topographic indices.

Spatially distributed hydrological models have been shown to be sensitive to DEM resolution (Zhang and Montgomery, 1994; Wolock and Price, 1994) both in horizontal and vertical measurement (Kenward et al., 2000). Chauby et al. (2005) indicated that finer resolution DEM cell sizes may result in improved output from the Soil and Water Assessment Tool (SWAT). The effect of DEM resolution on water quality modeling and calibration – specifically due to changes in delineated watersheds – was reported by Teegavarapu et al. (2006) using a Hydrologic Simulation Program FORTRAN (HSPF) model.

3. Data

3.1. Study area

The three watersheds used for this study are located in Idaho, U.S.A., and include: Dry Creek Experimental Watershed (DCEW), Reynolds Creek Experimental Watershed (RCEW) and Slate Creek Watershed (SCW), as shown in Fig. 1. These watersheds were chosen because of: 1) the availability of extensive high point density airborne LiDAR datasets; 2) the availability of 1 m aerial images and existing stream feature data used for creating reference stream networks; and 3) areas with distinct topographical (and hence hydrographical) characteristics which represent different steep watersheds in this area. We recognize that our results will not necessarily apply in broader flatter watersheds due, in part, to the inherent difficulty in extracting drainage areas and networks from flat terrain. A brief description of each watershed follows.

3.1.1. Dry Creek Experimental Watershed (DCEW)

DCEW is located within the Boise Mountains in Southwestern Idaho (about 43° latitude, −116° longitude). DCEW includes the 28 km^2 northeastward trending Dry Creek drainage extending from 1000 to 2100 m in the granitic region of the Boise Front.

3.1.2. Reynolds Creek Experimental Watershed (RCEW)

RCEW, typical of much of the intermountain region of the western United States (Seyfried and Wilcox, 1995) is a rangeland located in the Owyhee Mountains of southwestern Idaho, approximately 80 km southwest of Boise, Idaho, USA. The watershed ranges in elevation from 1101 to 2241 m and has 239 km^2 drainage area.

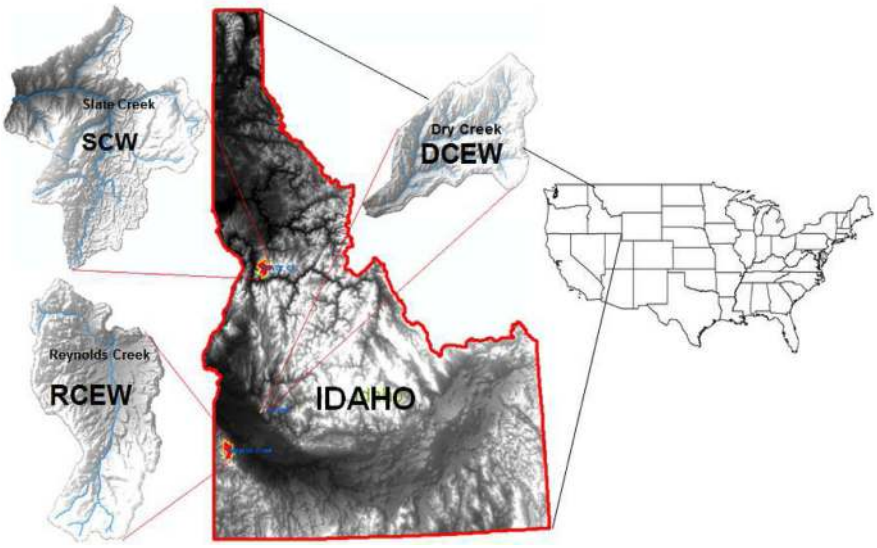

Fig. 1. Dry Creek Experimental Watershed (DCEW), Reynolds Creek Experimental Watershed (RCEW) and Slate Creek Watershed (SCW) in Idaho, USA.

3.1.3. Slate Creek Watershed (SCW)

SCW lies within the Salmon Basin in the southern part of Idaho's panhandle, and covers a total area of 320 km^2. Elevation within SCW ranges from 219 to 3843 m. Slate Creek originates high in the Boulder–White Cloud Mountains and descends northward to the Salmon River, descending nearly 2000 m.

3.2. Source data and accuracy

LiDAR data for RCEW and DCEW were acquired as part of a project using LiDAR for studying eco-hydrology and snow modeling, and data collection for SCW was commissioned by the USDA Forest Service. The LiDAR surveys were conducted by Watershed Sciences, Corvallis, Oregon. A Leica ALS50 Phase II LiDAR instrument was flown in a Cessna Caravan 208B aircraft over the period of September 29 to October 3, 2006 for SCW and November 10 to November 18, 2007 for RCEW and DCEW. The data were delivered in the LAS 1.1 file format with information on pulse return number, easting, northing, elevation, scan angle, and intensity for each return. The vendor-reported vertical absolute accuracy, represented as Root Mean Square Error (RMSE), is 0.026 m and 0.033 m for DCEW and RCEW, respectively, and 0.088 m for SCW. Based on the relationship between horizontal error and flight altitude (1/1100th), the horizontal accuracy is estimated at approximately 0.30 m.

3.3. LiDAR-based DEM creation

3.3.1. LiDAR data post-processing

Derivation of bare earth DEMs from raw LiDAR data requires removal of above-ground features such as vegetation and buildings. Since few buildings and bridges exist in the study areas, the main focus of filtering was to remove vegetation. The raw LiDAR point cloud was height-filtered to separate ground and non-ground returns described in Streutker and Glenn (2006). The non-ground return points were filtered by setting the canopy spacing (moving window) at 7 m, similar to other studies in the same and related ecosystems (Streutker and Glenn, 2006; Streutker et al., 2011; Glenn et al., 2011; Mitchell et al., 2011; Sankey and Glenn, 2011). The LiDAR data in this study were processed using Idaho State University's freely available open-source BCAL LiDAR Tools (http://bcal.geology.isu.edu/tools/lidar), which work with the free Interactive Data Language (IDL) virtual machine and as a plug-in for the image analysis software ENVI 4.7 (Exelis Visual Information Solutions, Boulder, Colorado, USA).

3.3.2. LiDAR DEM generation

LiDAR points are not evenly spaced, therefore, it is necessary to interpolate (where there are no existing points in the target raster cell) or to generalize (where there are many points in the target raster cell) to obtain a single value to be applied to each cell in the output raster DEM. After height-filtering the raw LiDAR data, DEMs were generated from the first returns using a hybrid natural neighbor interpolator (Tinkham et al., 2011). During the height-filtering process, the height of all vegetation returns above the bare-earth surface (interpolated using natural neighbors) was recorded. A bare-earth DEM was computed as the mean elevation of all the ground returns and elevation minus vegetation height of non-ground returns. For cells with no LiDAR returns, returns from neighboring pixels were used to compute the bare-earth elevation. A series of LiDAR-derived DEMs for DCEW at different cell sizes were generated based on the bare-earth LiDAR point cloud with all vegetation removed, are shown in Fig. 2. Resulting DEMs were then used for stream network delineation and hydrologic model application.

3.4. Stream network reference data

Assuming one dataset is the best available representation of a particular feature, we can estimate the relative error contained within other features by comparing them to the reference data (as a measure of relative accuracy). To create reference stream centerlines for the three study areas, field-derived stream networks and watershed boundary feature data were obtained for DCEW (Aishlin, 2007) and RCEW (Seyfried et al., 2001). A stream network feature dataset for SCW was retrieved from the National Hydrology Dataset (NHD) (http://nhd.usgs.gov/). These stream centerlines were checked and adjusted manually as needed using an imagery based verifying method (Pai and Saraswat, 2013) against 1 m digital orthoimagery of Idaho from 2009 National Agriculture Imagery Program (NAIP). NAIP imagery was not used as a sole source for stream network reference data because of vegetation obstructions in the imagery. Also, many stream segments in these high, arid watersheds are narrower than the 1 m pixel size of the NAIP data.

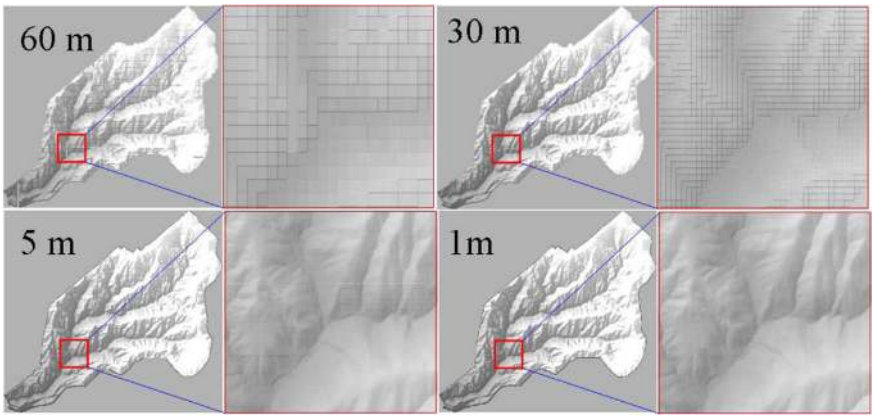

Fig. 2. LiDAR-derived DEM data at various resolutions for DCEW.

4. Analysis methods

4.1. Hydrographic features extraction

Techniques for extracting watershed boundaries and stream network hydrography from DEM data are well established (Beven and Kirkby, 1979; Jenson, 1991; Tarboton et al., 1991; Fekete et al., 2001; Teng et al., 2008; Wu et al., 2011; Schwanghart and Heckmann, 2012). We used geoprocessing tools within ArcGIS 9.3 (ESRI, Inc., Redlands, California), assembled in the ArcGIS ModelBuilder tool, to extract stream networks and watershed areas from each of the LiDAR-derived DEMs.

Hydrologic terrain analysis typically requires that the input DEM be projected into a local or regional geographic projection system that preserves distance and area measurements. For the purposes of this study, the North American Datum 1983 Universal Transverse Mercator (Zone 11 North) projection was used for all DEMs. We used a simple pit-filling technique where areas of low elevation are raised to the neighboring values, such that every DEM cell can effectively "flow out" of the grid.

Flow direction was computed using an 8-direction pour point model. The more computationally intensive D∞ method (Tarboton et al., 1991) was also explored but was not used because it produced essentially the identical results in our steep mountain watersheds. Flow accumulation was computed at every cell such that an area threshold could be set whereby any cells with an accumulation area higher than the threshold are defined as streams. The same area threshold (0.78 km^2) was used for all data to ensure a similar number of stream segments regardless of DEM resolution. Using map algebra to identify cells exceeding the accumulation threshold, stream networks were delineated from the DEM. Stream outlet points were used to identify drainage outlets of watershed areas. Raster-to-polyline and raster-to-polygon conversions were used to convert stream networks and watershed areas into a vector data format for comparison to reference data.

4.2. Feature accuracy assessment

Fig. 3 shows an example of multiple stream networks delineated from DEM data within a watershed and compared to reference data.

Three measurements were adopted to assess the difference between modeled and reference hydrography including total assessment of stream length; assessment of variation along the stream network; and assessment of sinuosity in resulting stream networks as described below.

4.2.1. Stream length

Total stream length of all stream segments in the watershed is used here as a measure of the level of stream detail as suggested in Day (1977). Total watershed or catchment area is often used as a critical parameter in hydrologic and water resources simulation models. This follows Callow et al. (2007) who used stream length and catchment area to explore the impact of hydrological correction methods on resulting DEMs.

4.2.2. Longitudinal root mean square error (LRMSE)

Longitudinal root mean square error (LRMSE) is defined as root mean square error (RMSE) computed between a number of paired sets of points located along both the modeled and reference stream networks (Fig. 4). LRMSE is used here as a measure of how accurately the modeled stream networks match the reference networks. The smaller the LRMSE, the closer the fit between modeled and reference data (Anderson et al., 2014).

Calculation of LRMSE was implemented by first dividing the reference line into m equal-length segments and n evenly spaced points, where $m = n - 1$. Then, for each of these points, the distance (d) from that point on the reference line to the nearest point on the line being compared, was determined. LRMSE was then calculated as:

$$\mathrm{LRMSE} = \mathrm{sqrt}\left\{\sum_i \left[d_i^2\right] / n\right\} \quad (1)$$

with $m = 100$ and $n = 101$.

4.2.3. Sinuosity

Sinuosity is used to describe the condition of curving in shape and is used here as a quantitative index of stream meandering and a distinctive property of channel pattern. Stream sinuosity, is computed as the ratio of channel length to direct distance between the beginning and end of the stream and is used in the study of the geometry, dynamics, and dimensions of alluvial channels (Chorley et al., 1984). Sinuosity was computed for all segments of both the reference stream network and the modeled stream networks at each DEM resolution for each study watershed.

5. Feature extraction results

DEM cell size, total stream length and data file size computed for the three study watersheds at each DEM resolution are shown in Tables 1–3. Total stream length variation is represented in Fig. 5.

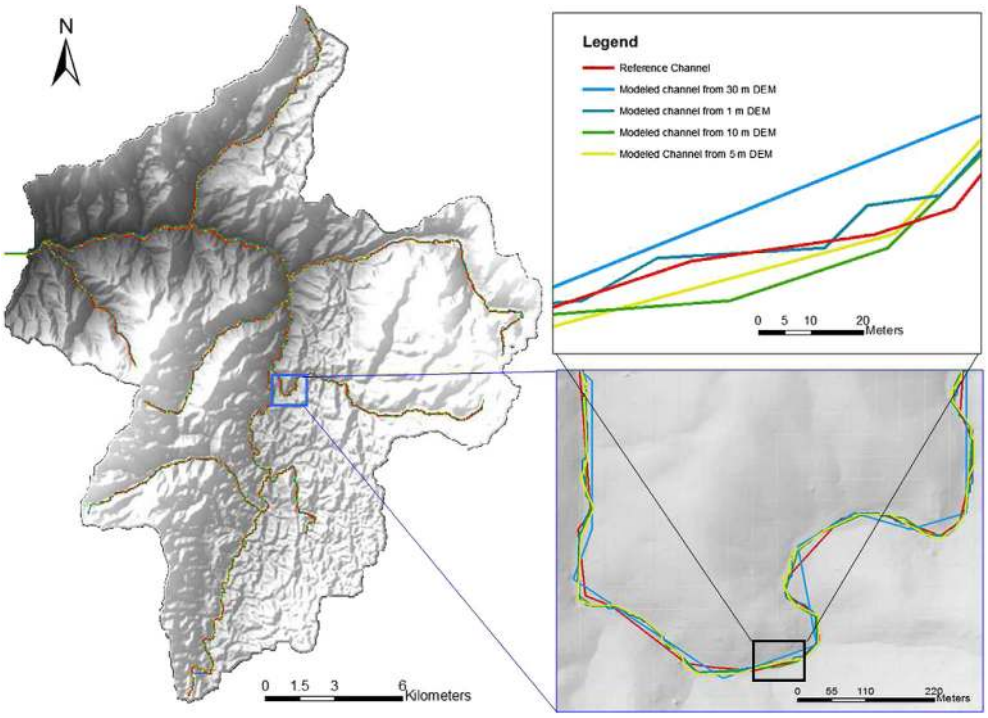

Fig. 3. A separate stream network was derived from each DEM and compared to reference data.

We observed a decreasing tendency in total stream length (Fig. 5) as a function of cell size in all three watersheds. This is consistent with the findings of Fekete et al. (2001) and may be due to the chosen re-gridding algorithms as noted by Wu et al. (2011). Resulting LRMSE values (as computed between modeled stream networks and reference stream) are shown in Fig. 6. LRMSE values were found to monotonically increase with increasing DEM cell size in the three study areas.

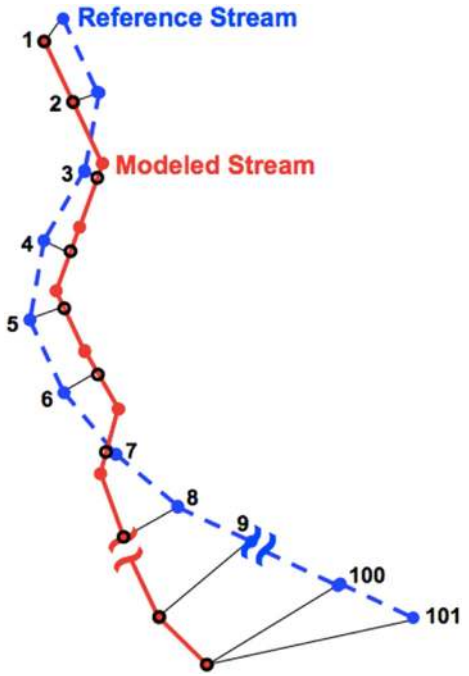

Fig. 4. Computation of LRMSE between modeled and reference stream segments.

The difference between the reference data and the derived streams in varying cell size ranged from 15 to 82 m for DCEW and from 20 to 39 m for RCEW and 21–99 m for SCW, respectively. The effect of varying cell size on LRMSE values was moderate at 1–10 m, with no more than 20% deviation from 1 to 10 m in all study areas. However, at 30 and 60 m, the LRMSE reaches as high as 99 m. The implications of this variability with respect to hydrologic modeling are discussed in the conclusions.

Compared to the sensitivity analysis of LRMSE, the sinuosity deviation from the reference with varying DEM cell size revealed an inverse tendency for cell sizes less than 10 m and an increase for cell sizes larger than 10 m (Fig. 7). The absolute sinuosity difference between the reference and the derived streams from varying cell-sized DEMs ranged from 0.05 to 0.1 for RCEW. At the cell size of 10 m, the absolute standard deviation value was smallest for each of the experimental watersheds, which indicates that stream networks derived from the cell sizes of 10 m were best matched to the reference stream.

6. Streamflow simulation and results

To examine the impact of DEM resolution on hydrologic modeling, streamflow was simulated using LiDAR DEMs at different resolutions at the DCEW outlet. DCEW was chosen due to its relatively small area and availability of observation data for calibrating the watershed model.

Table 1
RCEW hydrographic feature.

Cell size (m)	Data volume (kb)	Total stream length (m)
1	1,605,430	62,014
5	66,047	56,900
10	16,509	55,796
30	1836	52,657
60	460	51,647

Table 2
DCEW assessment.

Cell size (m)	Data volume (kb)	Total stream length (m)
1	267,637	39,798
5	10,710	35,521
10	2681	35,413
30	299	33,412
60	75	32,398

Table 3
SCW Assessment.

Cell size (m)	Data volume (kb)	Total stream length (m)
1	676,671	121,039
5	101,882	119,104
10	25,471	117,580
30	2832	112,311
60	709	100,550

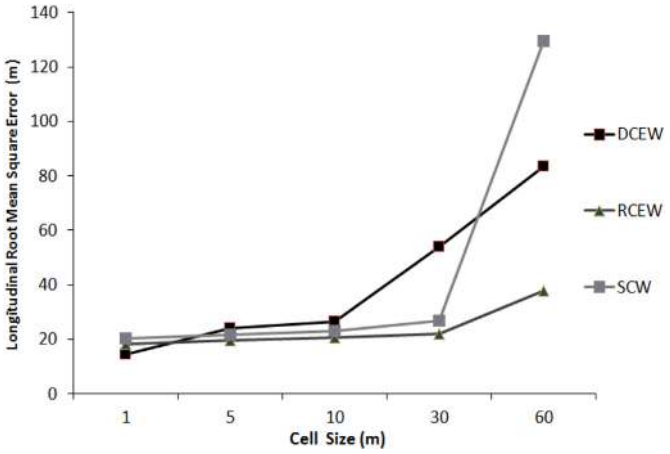

Fig. 6. LRMSE values as a function of DEM cell size for each watershed.

6.1. Hydrologic model calibration and validation

Hydrological Simulation Program – Fortran (HSPF) was used to simulate streamflow at DCEW outlet where observed data was available. HSPF is a continuous simulation model that represents hydrologic processes, storages and fluxes for a watershed. It is a comprehensive watershed model designed to simulate water quantity and quality processes and has been applied extensively to manage hydrologic and water quality issues in watersheds (Chew et al., 1991; Al-abed and Al-Sharif, 2008; Hall et al., 2008; Zhang and Montgomery 1994, Fonseca et al., 2014). Calibration of HSPF is an iterative procedure of parameter evaluation (Fig. 8), as a result of comparing simulated against observed values of interest.

We calibrated the DCEW watershed model using the HSPF parameter estimation software, HSPExp (Lumb et al., 1994). The system computes the following statistics from the simulated and observed streamflow time series: total runoff volume, mean of the low flow recession rates, mean of the lowest 50 percent and highest 10 percent of the daily mean flows, flow volumes for selected storms, seasonal volume and runoff volume for selected summer storms. It computes the ratio of simulated surface runoff and interflow volumes and the difference between the simulated actual evapotranspiration and the potential evapotranspiration.

The hydrological model was calibrated using flow and meteorological data acquired at the lower gage station using HydroDesktop (Ames et al., 2012) and via public ftp from the DCEW project located at the outlet of the DCEW watershed for the entire period of 2000–2005 and validated for a 3 year period (2007–2009). Potential evapotranspiration was derived from maximum and minimum air temperature with WDMUtil software, included in BASINS. During model calibration, values of several sensitive model parameters were varied within the acceptable and reasonable range to obtain the best practical agreement between observed and simulated streamflow data. Runoff responses to precipitation events were calibrated by adjusting various pervious land segment parameters PWATER: Lower Zone Evapotranspiration, Lower Zone Nominal Soil Moisture Storage, Index of Infiltration Capacity, Base Groundwater Recession, Fraction of Groundwater Inflow to Deep Recharge, Fraction of Remaining Evapotranspiration from Baseflow, Interflow Inflow Parameter, Interflow Recession Parameter and Upper Zone Nominal Soil Moisture Storage. The different DEMs used in simulation will differ in the channel routing geometry, channel length, width, depth, slope, surface area and volume of water. These values are obtained from the DEM's and are used to populate the hydraulic function tables in HSPF which will define the river reaches hydrology.

The performance evaluation of hydrologic models is generally made and reported through comparisons of simulated and observed variables. In our study, simulated and measured streamflow were used in statistical performance functions to compare catchments at the lower gage station. Three model efficiency criteria were applied for analyses: deviation of runoff volumes, Nash–Sutcliffe coefficient of efficiency and coefficient of determination.

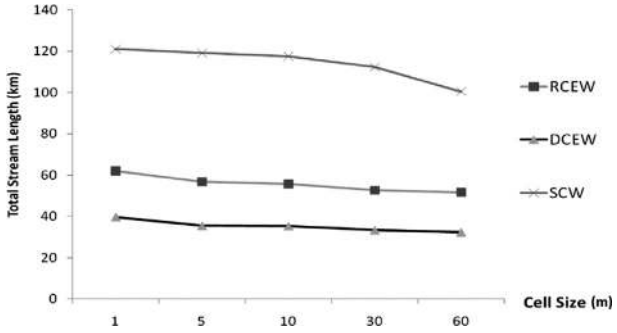

Fig. 5. Stream length as a function of cell size in the three watershed study areas.

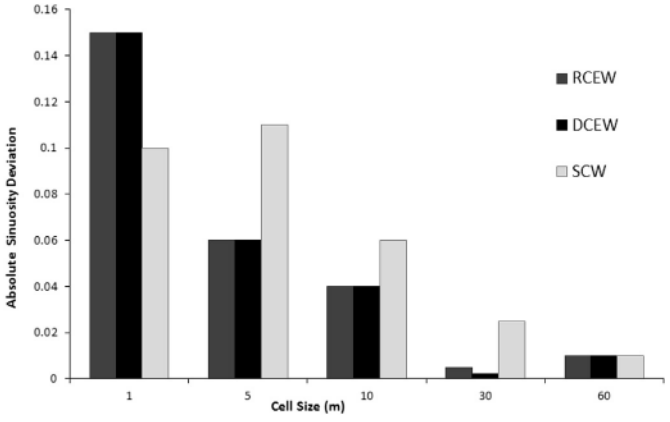

Fig. 7. Sinuosity difference by cell size in the three watershed study areas.

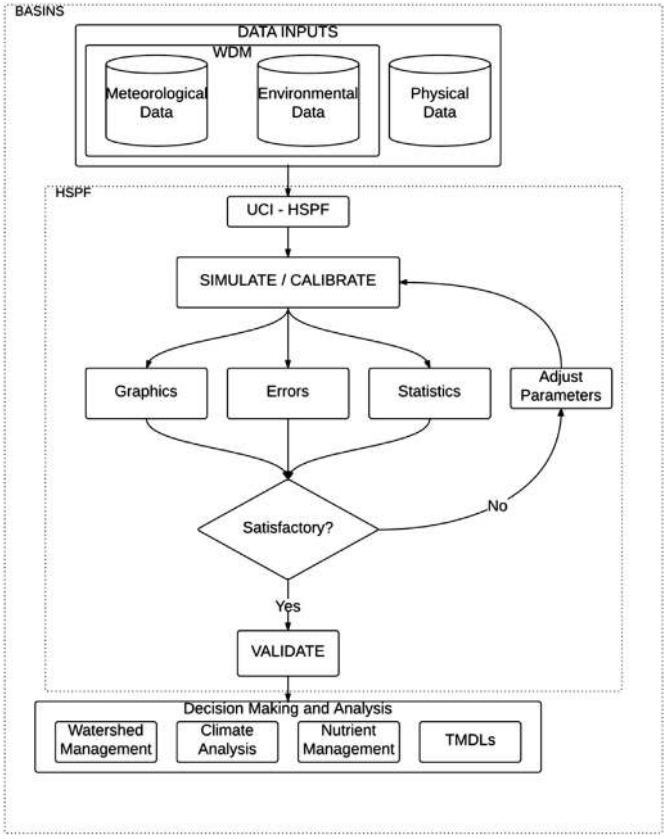

Fig. 8. HSPF calibration steps.

6.2. Model performance evaluation

To quantify model performance, several statistical measures were calculated for all simulations. Bennett et al. (2013) presents several methods for measuring quantitative performance including: direct model comparison, comparison of real and modeled values concurrently, key residual criteria, residual methods using data transformations and, correlation and model efficiency performance measures. A brief description of the statistical criteria used follows:

The deviation of runoff volumes *Dv*, also known as the percentage bias, is the simplest goodness-of-fit criterion (Legates and McCabe, 1999). Its value is calculated as follows:

$$Dv[\%]^n = \frac{\sum_{i=1}^{n}(S_i - O_i)}{\sum_{i=1}^{n}(O_i)} \times 100 \tag{2}$$

where S_i is the simulated discharge for each time step, O_i is the observed value and n is the total number of values within the period of analysis. For a perfect model, *Dv* is equal to zero. The smaller the *Dv* value, the better the performance of the model.

The Nash–Sutcliffe coefficient (Nr or E) is a measure of statistical association, which indicates the percentage of the observed variance that is explained by the model. The Nash–Sutcliffe coefficient (Nash and Sutcliffe, 1970), also known as the efficiency criterion (E), is estimated using Equation (3):

$$\mathrm{E} = 1 - \frac{\sum_{i=1}^{n}(O_i - S_i)^2}{\sum_{i=1}^{n}(O_i - \varnothing_i)^2} \tag{3}$$

where $\varnothing_i$ is the average measured discharge and all the other variables have the same meaning as above. The second term in Equation (3) represents the ratio between the mean square error (MSE) and the variance of the observed data. Thus, if a value of *E* equals to zero it indicates that the model output is not better than the averaged observed streamflow for the entire period of analysis. Essentially, the closer the model efficiency to 1, the more accurate the model. Mean Square Error (MSE) quantifies the difference between values implied by an estimator and the true values of the quantity being estimated, a value of zero means that the estimator predicts observations of the parameter with perfect accuracy. It can be estimated by using Equation (4):

$$\mathrm{MSE} = \frac{1}{n}\sum_{i=1}^{n}(y_i - o_i) \tag{4}$$

where n is the number of predictions, y_i is the estimation values and o_i are the observed values.

Root Mean Square Error (RMSE) – also called root mean square deviation – is the standard deviation of the differences between predicted values by a model and the observed values. RMSE of a model prediction is defined in Equation (5):

$$\mathrm{RMSE} = \sqrt{\frac{1}{n}\sum_{i=1}^{n}(y_i - o_i)} \tag{5}$$

Fourth Root Mean Quadruple Error (R4MS4E) is a statistic that emphasizes large errors by using the fourth power of the RMSE as in Equation (6):

$$\mathrm{R4MS4E} = \sqrt[4]{\frac{1}{n}\sum_{i=1}^{n}(o_i - s_i)^4} \tag{6}$$

Relative Volume Error (RVE) gives an indication of how good a measurement is relative to the size of the sample being measured. RVE can vary between $-\infty$ and ∞ with an ideal value of zero; it is estimated using Equation (7):

$$\mathrm{RVE} = \frac{\frac{1}{n}\sum_{i=1}^{n}(o_i - s_i)}{\frac{1}{n}\sum_{i=1}^{n}(o_i)} \tag{7}$$

The Coefficient of Determination (R^2) determines how much the variance between two variables is described by a linear fit. It can vary between 0 and 1, the higher the value the better fit (Equation (8)).

$$R^2 = \left(\frac{\sum_{i=1}^{n}(o_i - \varnothing)(y_i - \bar{y})}{\sqrt{\sum_{i=1}^{n}(o_i - \varnothing)^2} \times \sqrt{\sum_{i=1}^{n}(y_i - \bar{y})^2}}\right)^2 \tag{8}$$

where $\bar{y}$ is the average of the predicted values.

Standard Deviation Ratio (RSR) is similar to RMSE weighted by standard deviation of the observed values; with an ideal value of zero it can vary between zero and ∞ and is estimated using Equation (9):

$$\mathrm{RSR} = \frac{\sqrt{\sum_{i=1}^{n}(o_i - s_i)^2}}{\sqrt{\sum_{i=1}^{n}(o_i - \varnothing)^2}} \tag{9}$$

6.3. Hydrological simulation sensitivity based on DEM resolution

The values of hydrologic parameters that were adjusted using HSPExp during the calibration process are within the range of

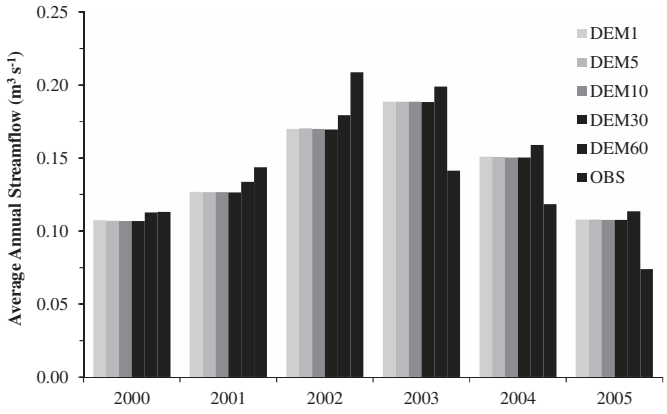

Fig. 9. Observed and model simulated annual streamflow data for the DCEW.

those shown in literature (Bicknell et al., 2005). Simulated annual streamflow for the different DEM resolutions for the period 2000 to 2005 is shown in Fig. 9. The total simulated runoff was overestimated for all DEMs, the percentage difference achieved was 6.2%, 6.1% 7.5%, 5.9% and 10.9% for 1 m, 5 m, 10 m, 30 m and 60 m resolutions respectively. There was good agreement between observed and simulated annual streamflow for the years 2000 and 2001 (<10% difference) and fair for the years 2002 and 2004 (<20%). Daily (Fig. 10) and average monthly (Fig. 11) hydrographs (DEM10) from the model were plotted with the respective observed discharge from the DCEW gaging station (daily and average monthly simulation for the remaining DEM's are available upon request). Daily and monthly calibration and validation shows fair results based on the statistics criteria shown in Table 4.

For validation purposes, the calibrated model was run for 2007–2009 without changing any parameter values. Simulated daily and average monthly, were compared with respective observed data values. Fig. 12 and Fig. 13 show the results obtained for the 10 m DEM resolution.

Satisfactory agreement between observed and simulated streamflow was obtained in the validation model. The total simulated runoff was underestimated by 8.9% and 9% for daily and average monthly. Even though the Nash–Sutcliffe coefficient of efficiency value is considered to be a satisfactory modeling result for both calibration and validation it is worth noting that observed flow data for DCEW is affected by ice formation during winter months affecting data accuracy.

Results of this calibration and validation show that insignificant variations in model accuracy occur depending on the resolution of the input LiDAR-derived DEM used to generate stream networks and watershed boundaries. Although the largest deviation of runoff volume occurred for the 60 m cell size DEM, there is no consistent pattern in the simulation error based on the DEM used. We expect that the lack of apparent effect on model results may be due, in part, to the low temporal resolution of the model (daily and monthly time steps) and that a higher temporal resolution model might show more dramatic effects of DEM resolution.

7. Conclusions

The effect of LiDAR-derived DEM resolution on hydrographic features derivation is clearly evident. Among all the DEM samples from 1 to 60 m cell size, the total stream length were greatest at the cell size of 1 m, and there was a descending tendency with the increase in cell size. The results show that higher resolution LiDAR-derived DEMs produce more detailed hydrographic features. LRMSE increased with cell size, indicating better accuracy at higher resolution (smaller cell size). Results demonstrated that the difference in the spatial distance between the reference and modeled streams tended to be smaller with a finer resolution. Interestingly, this variability in LRMSE, did not translate into notable variation in

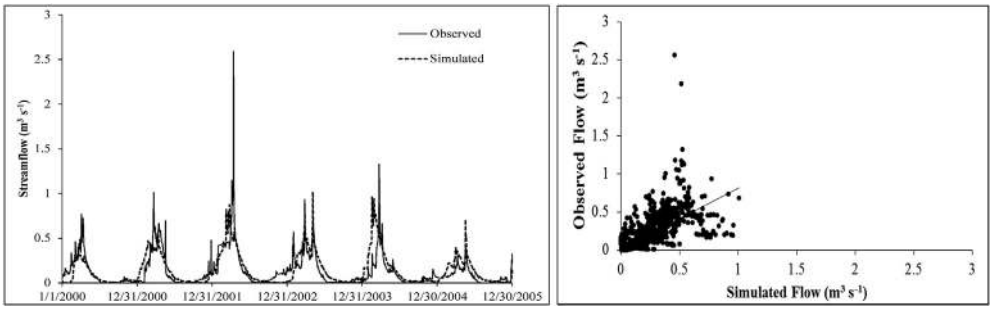

Fig. 10. Daily observed and simulated streamflow at DCEW lower station: time series (left) and scatter plot (right, $R^2 = 0.538$).

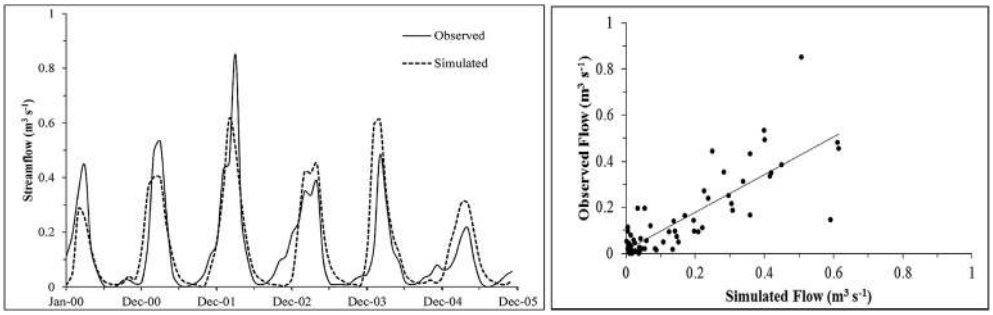

Fig. 11. Average monthly observed and simulated streamflow at DCEW lower station: time series (left) and scatter plot (right, $R^2 = 0.682$).

Table 4
Statistical criteria for the DCEW model calibration by DEM cell size.

	DEM1	DEM5	DEM10	DEM30	DEM60
Calibration					
Daily					
E	0.45	0.45	0.50	0.45	0.41
RSR	0.75	0.75	0.71	0.74	0.77
R^2	0.54	0.54	0.54	0.54	0.42
Dv (%)	6.20%	6.10%	7.50%	5.90%	10.90%
MSE	0.02	0.02	0.02	0.02	0.02
RMSE	0.14	0.14	0.13	0.14	0.14
R4MS4E	0.36	0.36	0.35	0.36	0.36
RVE	0.07	0.07	0.08	0.06	0.12
Monthly					
E	0.64	0.64	0.65	0.64	0.61
RSR	0.60	0.60	0.60	0.60	0.63
R^2	0.67	0.67	0.68	0.67	0.65
Dv (%)	6.30%	6.10%	7.40%	6.00%	11.00%
MSE	0.01	0.01	0.01	0.01	0.01
RMSE	0.10	0.10	0.10	0.10	0.10
R4MS4E	0.17	0.17	0.17	0.17	0.18
RVE	0.07	0.07	0.08	0.06	0.12
Validation					
Daily					
E	0.50	0.50	0.49	0.50	0.47
RSR	0.61	0.60	0.71	0.60	0.61
R^2	0.52	0.52	0.52	0.52	0.52
Dv (%)	−10.70%	−9.20%	−8.90%	−9.00%	−0.60%
MSE	0.01	0.01	0.01	0.01	0.01
RMSE	0.10	0.10	0.10	0.10	0.10
R4MS4E	0.18	0.18	0.18	0.18	0.17
RVE	−0.12	−0.10	−0.08	−0.10	−0.01
Monthly					
E	0.63	0.63	0.64	0.63	0.61
RSR	0.61	0.61	0.47	0.61	0.62
R^2	0.64	0.64	0.65	0.64	0.64
Dv (%)	−10.10%	−8.70%	−9.00%	−8.40%	−0.10%
MSE	0.01	0.01	0.01	0.01	0.01
RMSE	0.08	0.08	0.07	0.08	0.08
R4MS4E	0.12	0.12	0.11	0.12	0.11
RVE	−0.10	−0.09	−0.08	−0.08	0.00

hydrologic model results. We also observed that the absolute deviation between sinuosity of sample streams and reference data reached its smallest value at the cell size of 10 m. This demonstrates the resulting shape of streams obtained from LiDAR data matched best with the reference data at an intermediate cell size instead of the highest resolution (1 m DEM).

Although we based our study on LiDAR data, we expect that similar results would be achieved using DEM's derived from other data sources. These results are consistent with Zhang and Montgomery (1994) who proposed that a 10 m grid cell size represents a rational compromise between increasing resolution and data volume for simulating geomorphic and hydrological processes. This also agrees with Zhang et al. (2008) who showed that 10 m LiDAR DEM modeled watershed discharge and sediment yield were closest to field observations. Indeed, although extremely high-resolution data are becoming more readily available, our results show that the use of such data may not necessarily result in better DEMs for hydrologic applications.

Our daily and average monthly streamflow simulation modeling showed satisfactory agreement between observed and simulated values, evaluated by the Nash–Sutcliffe coefficient of efficient and confirmed by the model validation. Future work is needed to explore the sensitivity of the modeled streamflow using higher resolution DEM's at sub daily model time steps. Also, sources of inaccurate data due to frozen conditions and consequently reduced streamflow need to be further investigated in the DCEW watershed.

In summary, our results confirm that higher resolution LiDAR-generated DEMs generally do result in improved stream network and watershed boundary representations, but we determined that the improvements in hydrography do not necessarily result in improved streamflow simulations using a watershed scale hydrologic model. These results have significant implications for resource allocation in hydrologic modeling, as they suggest that expensive data collection efforts (e.g. LiDAR data collection) for the express purpose of generating high resolution DEMs for watershed

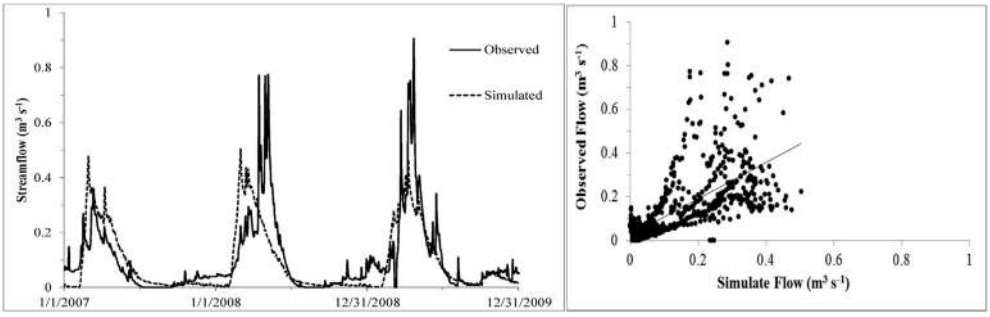

Fig. 12. Daily observed and simulated streamflow for the validated model at DCEW lower station: time series (left) and scatter plot (right, $R^2 = 0.519$).

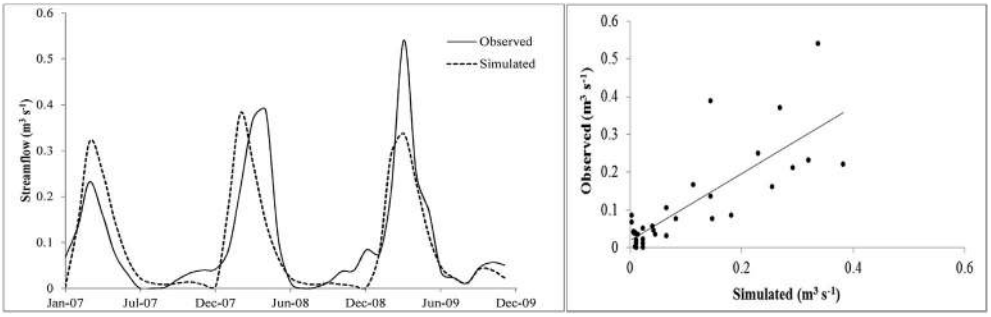

Fig. 13. Average monthly observed and simulated streamflow for the validated model at DCEW lower station: time series (left) and scatter plot (right, $R^2 = 0.654$).

modeling may not necessarily result in better hydrologic simulations.

Acknowledgments

The authors wish to give thanks to Dr. Jim McNamara for sharing data for use in this research and to the staff at BCAL for their LiDAR data processing training and technical support. This study has been supported in part by the National Science Foundation Idaho EPSCoR Program under award number EPS-814387 and by NOAA OAR Earth Systems Research Laboratory/Physical Sciences Division (ESRL/PSD) under award number NA09OAR4600221. André R. Fonseca acknowledges his doctoral fellowship (SFRH/BD/69654/2010) supported by FCT.

References

Agarwal, P.K., Arge, L., Danner, A., 2006. From point cloud to grid DEM: a scalable approach. In: Riedl, Andreas, Kainz, Wolfgang, Elmes, Gregory (Eds.), Progress in Spatial Data Handling, 12th International Symposium on Spatial Data Handling. Springer-Verlag, p. 771.

Aishlin, P., 2007. Groundwater Recharge Estimation Using Chloride Mass Balance, Dry Creek Experimental Watershed. MS Hydrological Sciences, Master's thesis. Boise State University.

Al-abed, N., Al-Sharif, M., 2008. Hydrological modeling of Zarqa river Basin – Jordan using the hydrological simulation program-FORTRAN (HSPF) model. Water Resour. Manag. 22, 1203–1220.

Ames, D.P., Horsburgh, J.S., Cao, Y., Kadlec, J., Whiteaker, T., Valentine, D., 2012. Hydrodesktop: web services-based software for hydrologic data discovery, download, visualization, and analysis. Environ. Model. Softw. 37, 146–156. http://dx.doi.org/10.1016/j.envsoft.2012.03.013.

Anderson, D.L., Ames, D.P., Yang, P., 2014. Quantitative methods for comparing different polyline stream network models, J. Geogr. Inform. Syst. 6 (2), 88–98 http://dx.doi.org/10.4236/jgis.2014.62010.

Bennett, N.D., Croke, B.F.W., Guariso, G., Guillaume, J.H.A., Hamilton, S.H., Jakeman, A.J., Marsili-Libelli, S., Newham, L.T.H., Norton, J.P., Perrin, C., Pierce, S.A., Robson, B., Seppelt, R., Voinov, A.A., Fth, B.D., Andreassian, V., 2013. Characterising performance of environmental models. Environ. Model. Softw. 40, 1–20.

Beven, K.J., Kirkby, M.J., 1979. A physically based, variable contributing area model of basin hydrology. Hydrol. Sci. Bull. 24, 43–69.

Bicknell, B., Imhoff, J., Kittle, J., Jobes, T., Donigian, A., 2005. Hydrological Simulation Program – FORTRAN: HSPF Version 12.2 User's Manual, Athens, GA.

Callow, J.N., Van Niel, K.P., Boggs, G.S., 2007. How does modifying a DEM to reflect known hydrology affect subsequent terrain analysis? J. Hydrol. 332 (1), 30–39.

Charrier, R., Li, Y., 2012. Assessing resolution and source effects of digital elevation models on automated floodplain delineation: a case study from the Camp Creek Watershed, Missouri. Appl. Geogr. 34, 38–46.

Chaubey, I., Cotter, A.S., Costello, T.A., Soerens, T.S., 2005. Effect of DEM data resolution on SWAT output uncertainty. Hydrol. Process. 19, 621–628.

Chew, C.Y., Moore, L.W., Smith, R.H., 1991. Hydrological simulation of Tennessee's north Reelfoot Creek watershed. Res. J. Water Pollut. Control Fed. 63, 10–16.

Chorley, R.J., Schumm, S.A., Sugden, D.E., 1984. Geomorphology. Methuen, London, p. 605.

Chow, E.T., Hodgson, M.E., 2009. Effects of LiDAR post-spacing and DEM resolution to mean slope estimation. Int. J. Geogr. Inf. Sci. 23 (10), 1277–1295.

Day, T.J., 1977. Observed mixing lengths in mountain streams. J. Hydrol. 35 (2), 125–136.

DeVantier, B.A., Feldman, A.D., 1993. Review of GIS applications in hydrologic modeling. J. Water Resour. Plan. Manag. 119, 246–261.

Farr, T.G., Kobrick, M., 2000. Shuttle radar topography mission produces a wealth of data. Am. Geophys. Union Eos 81, 583–585.

Fekete, B.M., Vörösmarty, C.J., Lammers, R.B., 2001. Scaling gridded river networks for macroscale hydrology: development, analysis, and control of error. Water Resour. Res. 37 (7), 1955–1967.

Fonseca, A., Ames, D.P., Yang, P., Botelho, C., Boaventura, R., Vilar, V., 2014. Watershed model parameter estimation and uncertainty in data-limited environments. Environ. Model. Softw. 51, 84–93.

Glenn, N.F., Spaete, L., Sankey, T., Derryberry, D., Hardegree, S., Mitchell, J., 2011. Errors in LiDAR-derived shrub height and crown area on sloped terrain. J. Arid Environ. 75 (4), 377–382.

Hall, K.M., Zeckoski, R.W., Brannan, K.M., 2008. FTABLE generation method effects on instream fecal bacteria concentrations simulated with HSPF. J. Am. Water Resour. Assoc. 44, 489–495.

Han, W., Di, L., Zhao, P., Shao, Y., 2012. DEM explorer: an online interoperable DEM data sharing and analysis system. Environ. Model. Softw. 38, 101–107.

Jenson, S.K., 1991. Applications of hydrological information automatically extracted from digital elevation models. Hydrol. Process. 5 (1), 31–44.

Jenson, S.K., Domingue, J.O., 1988. Extracting topographic structure from digital elevation data for geographic information system analysis. Photogramm. Eng. Remote Sens. 54, 1593–1600.

Kenward, T., Lettenmaier, D.P., Wood, E.F., Fielding, E., 2000. Effects of digital elevation model accuracy on hydrologic predictions. Remote Sens. Environ. 74 (3), 432–444.

Kienzle, S., 2004. The effect of DEM raster resolution on first order, second order and compound terrain derivatives. Trans. GIS 8 (1), 83–111.

Kinsey-Henderson, A.E., Wilkinson, S.N., 2013. Evaluating Shuttle radar and interpolated DEMs for slope gradient and soil erosion estimation in low relief terrain. Environ. Model. Softw. 40, 128–139.

Kraus, K., Pfeifer, N., 2001. Advanced DTM generation from LIDAR data. Int. Arch. Photogramm. Remote Sens. Spatial Inf. Sci. 34 (3/W4), 23–30.

Legates, D.R., McCabe Jr., G.J., 1999. Evaluating the use of "goodness-of-fit" measures in hydrologic and hydroclimatic model validation. Water Resour. Res. 35 (1), 233–241 http://dx.doi.org/10.1029/1998WR900018.

Lumb, Alan M., McCammon, Richard B., John, L., Kittle Jr., , 1994. User's Manual for an Expert System (HSPEXP) for Calibration of the Hydrological Simulation Program – FORTRAN. U.S. Geological Survey, Reston, VA.

Mitchell, J., Glenn, N.F., Sankey, T., Derryberry, D.R., Anderson, M.O., Hruska, R., 2011. Small-footprint LiDAR estimations of sagebrush canopy characteristics. Photogramm. Eng. Remote Sens. 77 (5), 521–530.

Moore, I.D., 1991. Digital terrain modeling in hydrology. Hydrol. Process. 5 (1), 3–30.

Murphy, P.N.C., Ogilvie, J., Meng, F., Arp, P., 2007. Stream network modeling using lidar and photogrammetric digital elevation models: a comparison and field verification. Hydrol. Process. 22 (12), 1747–1754.

Nash, J.E., Sutcliffe, J.V., 1970. River flow forecasting through conceptual models, part I – a discussion of principles. J. Hydrol. 10, 282–290.

Olivera, F., 2001. Extracting hydrologic information from spatial data for HMS modeling. J. Hydrol. Eng. 6, 524–530.

Pai, N., Saraswat, D., 2013. A geospatial tool for delineating streambanks. Environ. Model. Softw. 40, 151–159.

Sankey, T., Glenn, N., 2011. Landsat-5 TM and lidar fusion for sub-pixel Juniper Tree cover estimates in a western rangeland. Photogramm. Eng. Remote Sens. 77 (12).

Schwanghart, W., Heckmann, T., 2012. Fuzzy delineation of drainage basins through probabilistic interpretation of diverging flow algorithms. Environ. Model. Softw. 33, 106–113.

Seyfried, M., Wilcox, B.P., 1995. Scale and the nature of spatial variability: field examples and implications to hydrologic modeling. Water Resour. Res. 31, 173–184.

Seyfried, M., Harris, R., Marks, D., Jacob, B., 2001. Geographic database, Reynolds creek experimental watershed, Idaho, United States. Water Resour. Res. 37 (11), 2825–2829.

Shore, M., Murphy, P.N.C., Jordan, P., Mellander, P.E., Kelly-Quinn, M., Cushen, M., Melland, A.R., 2013. Evaluation of a surface hydrological connectivity index in agricultural catchments. Environ. Model. Softw. 47, 7–15.

Sørensen, R., Seibert, J., 2007. Effects of DEM resolution on the calculation of topographical indices: TWI and its components. J. Hydrol. 347 (12), 79–89.

Streutker, D., Glenn, N.F., 2006. LiDAR measurement of sagebrush steppe vegetation heights. Remote Sens. Environ. 102, 135–145.

Streutker, D.R., Glenn, N.F., Shrestha, R., 2011. A slope-based method for matching elevation surfaces. Photogramm. Eng. Remote Sens. 77 (7), 743–750.

Tarboton, D.G., Ames, D.P., 2001. Advances in the mapping of flow networks from digital elevation data. In: World Water and Environmental Resources Congress. Am. Soc Civil Engrs, USA, pp. 20–24.

Tarboton, D.G., Bras, R.L., Rodriguez-Iturbe, I., 1991. On the extraction of channel networks from digital elevation data. Hydrol. Process. 5 (1), 81–100.

Teegavarapu, Ramesh S.V., Viswanathan, C., Lindell, O., 2006a. Effect of digital elevation model (DEM) resolution on the hydrological and water quality modeling. In: Proceedings of the World Environmental and Water Resources Congress 2006 http://dx.doi.org/10.1061/40856(200)216.

Teegavarapu, R.S., Viswanathan, C., Ormsbee, L., 2006b. Effect of digital elevation model (DEM) resolution on the hydrological and water Quality Modeling. In: Proceedings of the World Environmental and Water Resources Congress 2006 http://dx.doi.org/10.1061/40856(200)216.

Teng, J., Vaze, J., Tuteja, N.K., Gallant, J.C., 2008. A GIS-based tool for spatial and distributed hydrological modelling: CLASS spatial analyst. Trans. GIS 12 (2), 209–225.

Tesfa, T.K., Tarboton, D.G., Watson, D.W., Schreuders, K.A.T., Baker, M.E., Wallace, R.M., 2011. Extraction of hydrological proximity measures from DEMs using parallel processing. Environ. Model. Softw. 26 (12), 1696–1709.

Tinkham, W.T., Huang, H., Smith, A.M.S., Shrestha, R., Falkowski, M.J., Hudak, A.T., Link, T.E., Glenn, N.F., Marks, D., 2011. A comparison of two open source lidar surface classification algorithms. Remote Sens. 3 (3), 638–649.

Vaze, J., Teng, J., Spencer, G., 2010. Impact of DEM accuracy and resolution on topographic indices. Environ. Model. Softw. 25 (10), 1086–1098.

Wolock, D.M., Price, C.V., 1994. Effects of digital elevation model map scale and data resolution on a topography-based watershed model. Water Resour. Res. 30 (11), 3041–3052.

Wu, H., Kimball, J.S., Mantua, N., Stanford, J., 2011. Automated upscaling of river networks for macroscale hydrological modeling. Water Resour. Res. 47 (3).

Xiaoye, L., 2008. Airborne LiDAR for DEM generation: some critical issues. Prog. Phys. Geogr. 32 (1), 31–49.

Zhang, W., Montgomery, D.R., 1994. Digital elevation model grid size, landscape representation, and hydrologic simulations. Water Resour. Res. 30, 1019–1102.

Zhang, J.X., Chang, K.T., Wu, J.Q., 2008. Effects of DEM resolution and source on soil erosion modeling: a case study using the WEPP model. Int. J. Geogr. Inf. Sci. 22, 925–942.